Damaged cable identification in cable-stayed bridge from bridge deck strain measurements using support vector machine

Jianying Ren[a,b] , Bing Zhang[c] , Xinqun Zhu[c], Shaohua Li[a]

[a] *State Key Laboratory of Mechanical behavior and System Safety of Traffic Engineering Structures, Shijiazhuang Tiedao University, Shijiazhuang Hebei, 050043, China*

[b]*Department of Engineering Mechanics, Shijiazhuang Tiedao University, Shijiazhuang Hebei, 050043, China*

[c]*School of Civil and Environmental Engineering, University of Technology Sydney, Broadway, NSW 2007, Australia*

Abstract: A new two-step approach is developed for damaged cable identification in a cable-stayed bridge from deck bending strain responses using Support Vector Machine (SVM). A Damaged Cable Identification Machine (DCIM) based on support vector classification is constructed to determine the damaged cable and a Damage Severity Identification Machine (DSIM) based on support vector regression is built to estimate the damage severity. A field cable-stayed bridge with a long-term monitoring system is used to verify the proposed method. The three-dimensional Finite Element Model (FEM) of the cable-stayed bridge is established using ANSYS, and the model is validated using the field testing results, such as the mode shape, natural frequencies and its bending strain responses of the bridge under a moving vehicle. Then the validated FEM is used to simulate the bending strain responses of the longitude deck near the cable anchors when the vehicle is passing over the bridge. Different damage scenarios are simulated for each cable with various severities. Based on damage indexes vector (DIV), the training datasets and testing datasets are acquired, including single damaged cable scenarios and double damaged cable scenarios. Eventually, DCIM is trained using Support Vector Classification Machine (SVCM) and DSIM is trained using Support Vector Regression Machine (SVRM). The testing datasets are input in DCIM and DSIM to check their accuracy and generalization capability. Different noise levels including 5%, 10%, 20% are considered to study their anti-noise capability. The results show that DCIM and DSIM both have good generalization capability and anti-noise capability.

Keywords: damage identification, bending strain, support vector machine (SVM), finite element model, cable-stayed bridge

1. Introduction

Cable-stayed bridges are widely used all around the world. In this type of bridges, cables as the crucial components transfer the dead loads and live loads from the deck to the pylons. However, in practice, the cables are prone to deterioration and damage because of fatigue and corrosion (Mehrabi,

2006; Sun et al., 2013). Compared with other bridge components in the cable-stayed bridge, the cable is more vulnerable and usually has a shorter life. Therefore, in order to obtain the cable service state and ensure the safety of the bridge operation, cable monitoring has become an indispensable part of structural health monitoring (SHM) for cable-stayed bridges (Dong et al., 2018).

In cable-stayed bridges, the cable forces are usually considered as a significant safety indicator in monitoring process. Most of the cable monitoring approaches are to obtain the cable forces through various ways to evaluate the damage state of the cables, such as pressure gauge method, classical sensors method (Brice et al., 2008), vibration frequency method (Cho et al., 2010; Sim et al., 2014; Arjomandi et al., 2019; Huang et al. 2018; Ren et al., 2019), fiber bragg grating (FBG) method (Li et al., 2009), acoustic emission technology (AET) (Zejli et al., 2012; Li et al., 2011), vision-based monitoring method (Kim et al., 2013; Kim et al., 2017). Although these methods can obtain the cable tension forces, there are some limitations in practical applications. For instance, the method based on the cable fundamental vibration frequency is limited to long cables. The weak survivability and high cost of the smart cables with FBG-fiber make it not widely used. The accuracy of image-processing-based method is greatly affected by weather conditions.

In recent years, a few researchers utilize bridge deck strains, deck deflections, vertical dynamic displacements, deck shear forces, rotation influence lines to indirectly monitor the cable state. A method of detecting multiple damage in a cable-stayed bridge from the vertical dynamic of a vehicle crossing the bridge was presented by Yin and Tang (2011). It is difficult to measure the relative vehicle displacement in practice. The distributed strains along the bridge deck and the changes in support reactions are used by Nazarian et al. (2016a; 2016b) to detect the loss of cable forces, and then localize and quantify the damage in the cables. The laboratory and numerical results have been used to verify the proposed method. The partial cable damage using the abnormal variation of temperature-induced deck deflection caused by the cable damage was localized and quantified by Wang and Ye (2019). A cable damage identification technique based on the concept of rotation influence line (*RIL*) at the bridge bearing locations, and solely relies on measurements obtained from two points at either end of the bridge e.g., RIL_R and RIL_L was proposed by Alamdari et al. (2019). It is found that the cable damaged state will affect the bridge responses whether the bridge is under dead loads or live loads or temperature changes, and these indirect methods can identify the cable damage and bridge deck damage simultaneously. But most methods need to close traffic, which is difficult for bridges on traffic arteries. As the above, the operational environment has a significant effect on the identified results and it is limited the practical application.

Currently, with the development of artificial intelligence (AI), many researchers have introduced AI into structure damage identification or damage detection ways and have achieved many good results. Damage identification is formulated as an optimization problem, Ghannadi et al. (2019a 2019b 2020a 2020b) used Moth-Flame Optimization (MFO), Salp Swarm Algorithm (SSA), Multiverse Optimizer (MVO), and the grey wolf optimization to identify the damage severities and locations of space truss and steel frame. Ghannadi et al. (2019c 2021) also used artificial neural network (ANN) to detect the damage of skeletal structures. A two-step damage identification method combining a multilayer neural network and novelty detection is developed to robustly distinguish damage occurrence and severity regardless of temperature variations and noise perturbations by Gu et al. (2017). A graph neural network (GNN) framework is trained by the Message Passing Neural Network (MPNN) to identify damaged cables and estimate the cable cross-sectional areas by Son et al. (2021). A fully convolutional network called Ci-Net for structural crack identification based on Pixel-level labeled image training data is proposed by Ye et al. (2019).

Among different AI techniques, SVM is one of the youngest machine learning method, which is proposed by Vapnik (1998). The most remarkable characterization of SVM is the high potential of generalizing datasets whose number is small in the training stage and SVM does not get stuck in local optimum like artificial neural networks (Najafzadeh et al. 2020). So SVM have ever applied in solving various problems, such as scour prediction (Najafzadeh et al. 2016), prediction of oxygen demand (Najafzadeh et al. 2019b), environmental evaluation (Najafzadeh et al. 2019b), face detection, character recognition, three-dimension body recognition, remote sensing image analysis, etc. For these advantages and widely application, SVM is also used in the field of damage detection and structural identification (Hasni et al. 2017). Least squares support vector machine (LS-SVM) and incomplete static responses of a damaged structure are used to detect structural damage by Kourehli (2017). SVM was employed as a classifier to evaluate the capability of feature selection techniques toward improving the damage identification performance of the cable-stayed bridge by Bisheh et al. (2020). SVM classifiers were developed to fuse the clustered features and identify multiple damage states by Hasni et al. (2017). A framework was developed for data-driven structural diagnosis and damage detection using SVM by Pan et al. (2018). PSO-SVM classification model was employed to automatically identify longitudinal crack, transverse crack, surface corrosion, and pothole defect by Li et al. (2020). The bridge deck's deformation is mainly the bending deformation under moving vehicle loads, and the bending strains can be easily measured with less error using strain sensors. Furthermore, few researchers regard the problem of cable damage identification as a problem of classification and regression.

The aim of this study is to develop a novel method to estimate the cable state using SVM from the bending strain changes under moving vehicle loads. The analytical formulations between the damaged cable force and the bridge deck bending strains are established firstly using the finite element model. Then, a novel two-step cable damage identification approach is proposed: the damaged cable identification and the cable damage severity prediction. In the first step, a damage index vector (DIV) is defined. The damaged cable identification is considered as a multiple classification problem, and Support Vector Classification Machine (SVCM) is used to train the Damaged Cable Identification Machine (DCIM). In the second step, the damage severity identification of the cable is conducted and it is a nonlinear regression problem. Support Vector Regression Machine (SVRM) is utilized to train the Damage Severity Identifier Machine (DSIM). The proposed method is applied to a field cable-stayed bridge to identify single damaged cable and double damaged cables to verify its feasibility and effectiveness.

2 Damage identification approach

2.1 Support Vector Machine (SVM)

SVM is one of the effective supervised machine learning techniques in data classification and regression (Pan et al. 2018). As shown in Fig. 1, the key point of SVM is using the kernel function to transform the nonlinear problem in the original space into a linear problem in a higher dimensional feature space. Various kernel functions can be used, such as the linear, polynomial, or Gaussian RBF. In SVCM, a hyperplane is used to separate the two different classes of samples by maximizing the "margin", which is the double distance from the hyperplane to the closest data points in either class (Pan et al. 2018), shown in Fig.1(a). In SVRM, a hyperplane is used to fit the function by minimizing ε, which is the distance of the hyperplane moving up and down along the vertical axis, and all training points are between the two dotted lines, shown in Fig.2(b). Detailed information is given in the book by Vapnik (1998).

In this study, the SVM toolbox in Matlab is used to train the cable damage identification machines. The following sections will describe the details.

2.2 The cable-stayed bridge

In this paper, a field cable-stayed bridge over the Great Western Highway in the state of New South Wales, Australia was used as a case study to test and validate the proposed method. Fig.2(a) shows an illustration of the bridge (Alamdari et al., 2019). The cable-stayed bridge has a single A-shaped steel tower with a composite steel-concrete deck. The bridge is composed of 16 stay cables with a semi-fan arrangement. The bridge span and the tower height are 46 and 33 m, respectively. The deck has a

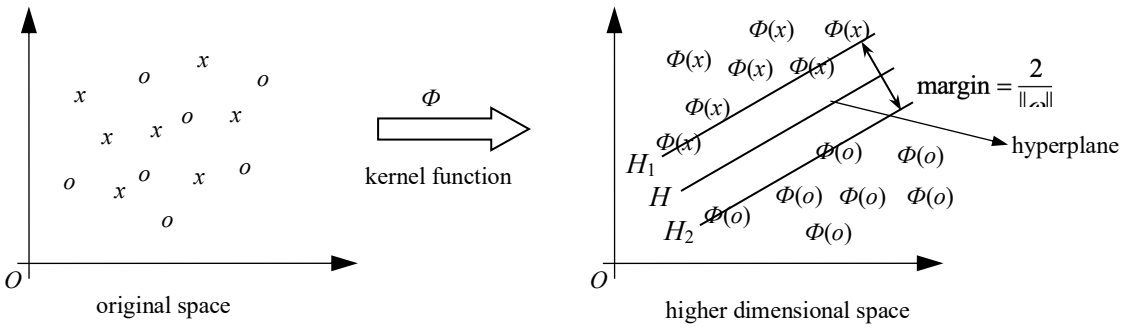

(a) SVCM

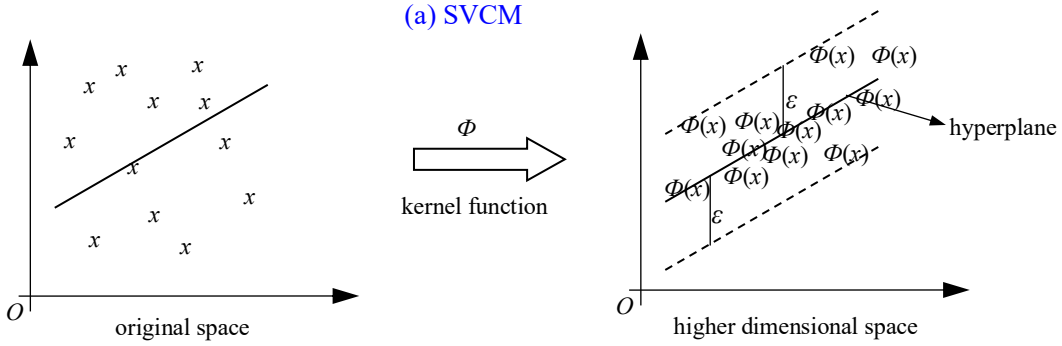

(b) SVRM

Fig.1 SVM basic idea diagram

(a) An illustration of the bridge

(b) The beam array

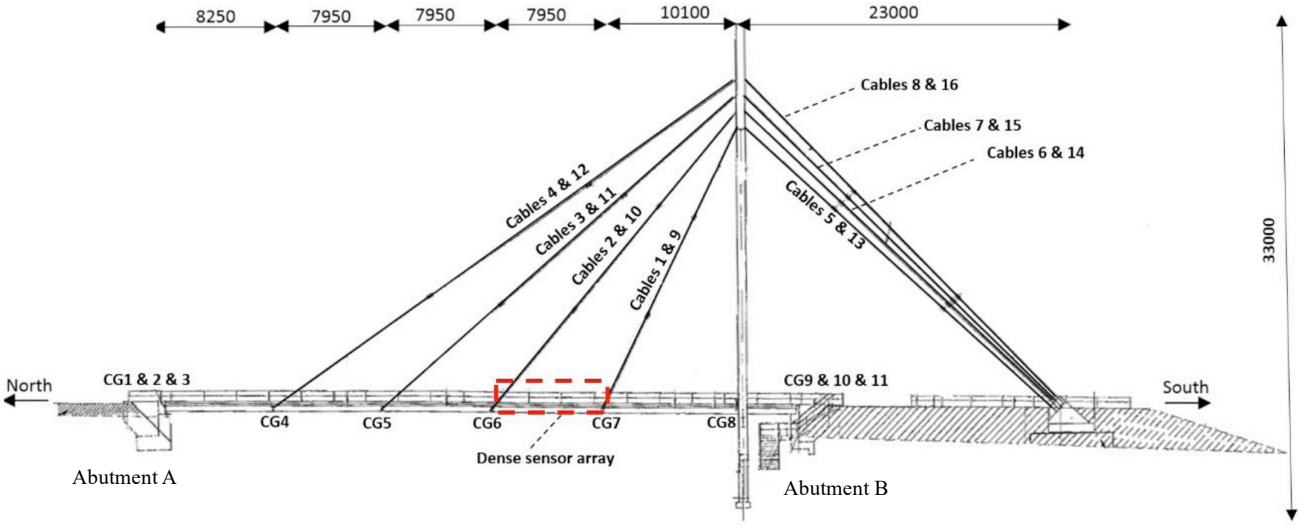

(c) Schematic view of the cable-stayed bridge

Fig.2 The real cable-stayed bridge

thickness of 0.16 m and a width of 6.3 m, and it is supported by four I-beam steel decks. These decks are internally attached by a set of equally spaced floor beams, as depicted in Fig.2(b). The assigned numbers

of the cables and the decks are shown in Fig.2 (c).

2.3 The relationship between the cable force and the bending strains of the bridge deck

Based on the aforementioned real cable-stayed bridge in the state of New South Wales, a simple plane calculation diagram shown in Fig.3(a) is employed for deriving the equations between the cable forces and the bridge deck bending strains. In practice, the cable forces change with the vehicle location x when it traveling on the bridge. To simplify the model, the cables can be removed and replaced by concentrated forces (Nazarian et al., 2016b), as shown in Fig.3(b). A roller support is used to represent the pylon to simplify the bridge as a continuous beam with two spans. Then the continuous beam is divided into six elements with seven nodes shown in Fig.3(b). The final calculation diagram is shown in Fig.3(c) with horizontal and vertical components of cable forces $F_{i\mathrm{h}}$ and $F_{i\mathrm{v}}$ as follows,

$$F_{i\mathrm{h}} = F_i \cos\theta_i \quad F_{i\mathrm{v}} = F_i \sin\theta_i \tag{1}$$

where, θ_i is the angle between the deck and the ith cable.

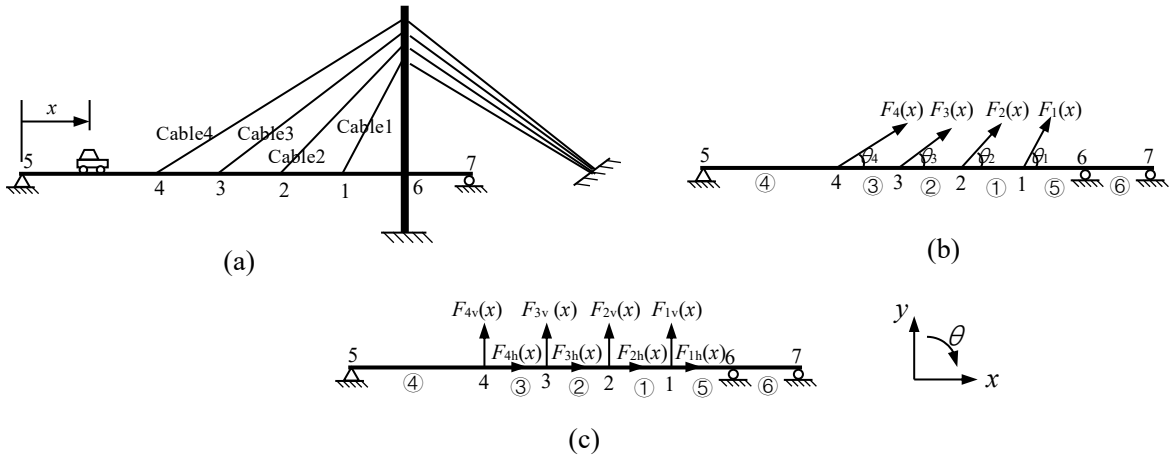

Fig.3 The cable-stayed bridge calculation diagram

The equilibrium equation can be obtained as follows:

$$F_{(x)} = K \cdot \Delta \tag{2}$$

where, F is the load vector,

$$F(x) = (F_{1\mathrm{h}}(x) \quad F_{1\mathrm{v}}(x) \quad 0 \quad F_{2\mathrm{h}}(x) \quad F_{2\mathrm{v}}(x) \quad 0 \quad F_{3\mathrm{h}}(x) \quad F_{3\mathrm{v}}(x) \quad 0 \quad F_{4\mathrm{h}}(x) \quad F_{4\mathrm{v}}(x) \quad 0 \quad \cdots \quad \ldots \quad 0 \quad 0 \quad 0 \quad 0 \quad 0)^{\mathrm{T}}_{1\times 17} \tag{3}$$

K is the beam stiffness matrix that has considered the boundary conditions,

$$K = \begin{bmatrix} k_{1,1} & \cdots & k_{1,17} \\ \vdots & \ddots & \vdots \\ k_{17,1} & \cdots & k_{17,17} \end{bmatrix} \tag{4}$$

where, $k_{i,j}$ is the stiffness coefficient, which means the ith load when the jth displacement equal to 1 and other displacements are all equal to 0. Δ is the nodes displacements vector,

$$\Delta(x) = (u_1(x) \quad v_1(x) \quad \varphi_1(x) \quad u_2(x) \quad v_2(x) \quad \varphi_2(x) \quad u_3(x) \quad v_3(x) \quad \varphi_3(x) \quad \cdots$$

$$\cdots \quad u_{4(x)} \quad v_{4(x)} \quad \varphi_{4(x)} \quad \varphi_{5(x)} \quad u_{6(x)} \quad \varphi_{6(x)} \quad u_{7(x)} \quad \varphi_{7(x)})_{1\times17}^{\mathrm{T}} \tag{5}$$

where, u_i, v_i and φ_i are the ith node horizontal displacement, vertical displacement and rotation displacement, respectively.

From Eq.(2), Δ can be obtained as

$$\Delta_{(x)} = K^{-1} \cdot F_{(x)} \tag{6}$$

where, K^{-1} is the inverse matrix of K as follows

$$K^{-1} = \begin{bmatrix} s_{1,1} & \cdots & s_{1,17} \\ \vdots & \ddots & \vdots \\ s_{17,1} & \cdots & s_{17,17} \end{bmatrix} \tag{7}$$

After obtaining the displacement of all nodes, each node's moment and bending strain can be obtained by analyzing the element. Here, element ⑥ is taken as an example to calculate the bending strain. The both ends force vector of element ⑥ can be represented as

$$\bar{F}_{(x)}^{\textcircled{e}} = \bar{K}^{\textcircled{e}} \cdot \delta_{(x)}^{\textcircled{e}} \tag{8}$$

where,

$$\bar{F}_{(x)}^{\textcircled{e}} = \left(F_{\mathrm{N}i(x)} \quad F_{\mathrm{s}i(x)} \quad M_{i(x)} \quad F_{\mathrm{N}j(x)} \quad F_{\mathrm{s}j(x)} \quad M_{j(x)}\right)^{\mathrm{T}} \tag{9}$$

where, $F_{\mathrm{N}i}$, $F_{\mathrm{N}j}$, $F_{\mathrm{s}i}$, $F_{\mathrm{s}j}$ and M_i, M_j are the axial forces, shearing forces and bending moments of the ith node and the jth node on element ⑥, respectively.

The stiffness matrix of element ⑥ is

$$\bar{K}^{\textcircled{e}} = \begin{bmatrix} k_{11} & k_{12} & k_{13} & k_{14} & k_{15} & k_{16} \\ k_{21} & k_{22} & k_{23} & k_{24} & k_{25} & k_{26} \\ k_{31} & k_{32} & k_{33} & k_{34} & k_{35} & k_{36} \\ k_{41} & k_{42} & k_{43} & k_{44} & k_{45} & k_{46} \\ k_{51} & k_{52} & k_{53} & k_{54} & k_{55} & k_{56} \\ k_{61} & k_{62} & k_{63} & k_{64} & k_{65} & k_{46} \end{bmatrix} \tag{10}$$

$\delta(x)^{\textcircled{e}}$ is the displacements of the ith node and the jth node on element ⑥,

$$\delta_{(x)}^{\textcircled{e}} = (u_{i(x)} \quad v_{i(x)} \quad \varphi_{i(x)} \quad u_{j(x)} \quad v_{j(x)} \quad \varphi_{j(x)})^{\mathrm{T}} \tag{11}$$

Then the bending strain ε_i can be obtained from the formula

$$\varepsilon_{i(x)} = \frac{M_{i(x)}y}{EI} \tag{12}$$

where, y is the distance from the neutral axis to the outmost cross-section fiber. E is the modulus of elasticity of the deck. I is the moment of inertia of the deck cross section.

Here, element ② is taken as an example to calculate the bending strains. If the local coordinate

system is consistent with the global coordinate system, the nodes' displacement vector of element ② is

$$\delta_{(x)}^{②} = (u_{3(x)} \quad v_{3(x)} \quad \varphi_{3(x)} \quad u_{2(x)} \quad v_{2(x)} \quad \varphi_{2(x)})^{\mathrm{T}} \tag{13}$$

Using Eq.(3), Eq.(6) and Eq.(7), $\delta_{(x)}^{②}$ can be obtained as following

$$\delta_{(x)}^{②} = S'F' = \begin{bmatrix} s_{71} & s_{72} & s_{74} & s_{75} & s_{77} & s_{78} & s_{7,10} & s_{7,11} \\ s_{81} & s_{82} & s_{84} & s_{85} & s_{87} & s_{88} & s_{8,10} & s_{8,11} \\ s_{91} & s_{92} & s_{94} & s_{95} & s_{97} & s_{98} & s_{9,10} & s_{9,11} \\ s_{41} & s_{42} & s_{44} & s_{45} & s_{47} & s_{48} & s_{4,10} & s_{4,11} \\ s_{51} & s_{52} & s_{54} & s_{55} & s_{57} & s_{58} & s_{5,10} & s_{5,11} \\ s_{61} & s_{62} & s_{64} & s_{65} & s_{67} & s_{68} & s_{6,10} & s_{6,11} \end{bmatrix} \begin{pmatrix} F_{1\mathrm{h}}(x) \\ F_{1\mathrm{v}}(x) \\ F_{2\mathrm{h}}(x) \\ F_{2\mathrm{v}}(x) \\ F_{3\mathrm{h}}(x) \\ F_{3\mathrm{v}}(x) \\ F_{4\mathrm{h}}(x) \\ F_{4\mathrm{v}}(x) \end{pmatrix} \tag{14}$$

where, F' is the cable force vector composed of non-zero forces, S' is the corresponding sub-matrix of K^{-1}.

Substituting Eq.(14) into Eqs.(8) and (12), ε_3 and ε_2 can be obtained as

$$\begin{pmatrix} \varepsilon_3(x) \\ \varepsilon_2(x) \end{pmatrix} = \begin{pmatrix} \frac{M_3(x)y}{EI} \\ \frac{M_2(x)y}{EI} \end{pmatrix} = BF' = \begin{pmatrix} B_{11} & B_{12} & B_{13} & B_{14} & B_{15} & B_{16} & B_{17} & B_{18} \\ B_{21} & B_{22} & B_{23} & B_{24} & B_{25} & B_{26} & B_{27} & B_{28} \end{pmatrix} \begin{pmatrix} F_{1\mathrm{h}}(x) \\ F_{1\mathrm{v}}(x) \\ F_{2\mathrm{h}}(x) \\ F_{2\mathrm{v}}(x) \\ F_{3\mathrm{h}}(x) \\ F_{3\mathrm{v}}(x) \\ F_{4\mathrm{h}}(x) \\ F_{4\mathrm{v}}(x) \end{pmatrix} \tag{15}$$

where,

$$B = \frac{y}{EI} \begin{pmatrix} k_{31} & k_{32} & k_{33} & k_{34} & k_{35} & k_{36} \\ k_{61} & k_{62} & k_{63} & k_{64} & k_{65} & k_{66} \end{pmatrix} \begin{bmatrix} s_{71} & s_{72} & s_{74} & s_{75} & s_{77} & s_{78} & s_{7,10} & s_{7,11} \\ s_{81} & s_{82} & s_{84} & s_{85} & s_{87} & s_{88} & s_{8,10} & s_{8,11} \\ s_{91} & s_{92} & s_{94} & s_{95} & s_{97} & s_{98} & s_{9,10} & s_{9,11} \\ s_{41} & s_{42} & s_{44} & s_{45} & s_{47} & s_{48} & s_{4,10} & s_{4,11} \\ s_{51} & s_{52} & s_{54} & s_{55} & s_{57} & s_{58} & s_{5,10} & s_{5,11} \\ s_{61} & s_{62} & s_{64} & s_{65} & s_{67} & s_{68} & s_{6,10} & s_{6,11} \end{bmatrix} \tag{16}$$

Eq.(15) shows the relationship between cable forces F' and the bending strains ε_3 and ε_2 of the bridge deck. From this equation, it can be found that each bending strain will change with the cable forces. This conclusion also applies to the three-dimensional model, but the expression is more complicated. It is well known that the cable forces are varied with different vehicle loads and different vehicle locations, and the bending strains of the bridge with the crossing vehicle are time-varying. When one of the cables is damaged, all cable forces will be redistributed and the corresponding bending strains can reflect the damage of the cables.

2.3 Damage identification approach

Damage in cables as a result of corrosion changes the cable cross-section and potentially mass per unit length (Huang et al., 2018). The cable damage will affect the cable tensile stiffness *EA,* furthermore

affect the cable tension forces. Therefore, in this paper, the cable damage is described using the cable tensile stiffness *EA* decreasing, and the damage severity is defined as,

$$de = \frac{EA_{\text{in}} - EA_{\text{da}}}{EA_{\text{in}}} \times 100\% \tag{17}$$

where, *de* is the cable damage severity, EA_{in} is the intact cable tensile stiffness, EA_{da} is the damaged cable tensile stiffness.

From the previous section, the bridge deck bending strains can reflect the damage of the cables, and are able to be measured easily with good accuracy. The DIV will be extracted from measured bending strains. However, the amount of strain data is very large because of the variation with vehicle location. In order to reduce the large amount of data, the maximum bending strains of the measured points are extracted as the main features of the data. For a beam structure, the position where the concentrated force act is usually the extreme point of the bending moment, and also the extreme point of the bending strain. In this study, the strain measurement points on the bridge deck are corresponding to eight cable anchors of the cable-stayed bridge. Then the damage identification index for each measurement point is defined as the difference between the maximum intact bending strain and the maximum damaged bending strain. DIV $\{X\}$ is obtained

$$\{X\} = (\Delta\varepsilon_1 \quad \cdots \quad \Delta\varepsilon_i \quad \ldots \quad \Delta\varepsilon_n)^{\text{T}} \tag{18}$$

where, $\Delta\varepsilon_i$ is the vector component at the *i*th measured point, and the index is calculated by

$$\Delta\varepsilon_i = \max(\varepsilon_{i\text{in}}) - \max(\varepsilon_{i\text{da}}) \tag{19}$$

where, $\max(\varepsilon_{i\text{in}})$ and $\max(\varepsilon_{i\text{da}})$are the maximum bending strains of intact bridge and damaged bridge at the *i*th measured point under the same vehicle load, respectively.

The cables are numbered and the damaged cable identification can be defined as a multi-class classification problem (MCP). It means that the number of categories will be *nc*, when the total number of the cables on cable-stayed bridge is *nc*. SVCM is a Multiple Classification Methods (MCM) and it can be used to train a DCIM, as the following function

$$\text{DCIM}(\{X\}) = \arg\max\{\text{sgn}(f_1(\{X\})), \quad \cdots, \quad \text{sgn}(f_{nc}(\{X\}))\} \tag{20}$$

where, $\{X\}$ is DIV. sgn($f_{nc}(X)$) is a two-class classifier, when $\{X\}$ is corresponding to the damaged cable of *nc*, sgn($f_{nc}(\{X\})$)=1, otherwise, sgn($f_{nc}(\{X\})$)=-1. DCIM($\{X\}$) equals the number of the damaged cable which is corresponding to the maximum of the two-class classifiers. So DCIM($\{X\}$) is a multi-class classifier. Consequently, the damaged cable can be identified by substituting any DIV into Eq.(20).

After determining the damaged cable, the next step is to identify the cable damage severity. The DSIM will be trained using the damage severity identification index datasets which only includes the

data of one damaged cable situation. Corresponding to the number of the bridge cables, the number of DSIMs should be *nc*, here it is sixteen. Because the damage severity is a continuous variable, it is impossible to prepare the training data corresponding all of the damage severity. The damage severities be 5%, 10%, 15%, 20%, etc. are used for the training data. Then the regression method (RM), SVRM, is utilized to train DSIMs. In DSIM, DIV$\{X\}$ is the independent variable and the damage severity *de* is the dependent variable. DSIM is a nonlinear higher dimensional function as,

$$de = \mathrm{DSIM}_{ic}(\{X\}) = \{\mathrm{A}\} \cdot \{X\} + b \tag{21}$$

where, $\mathrm{DSIM}_{ic}(\{X\})$ is for damaged cable *ic*, $\{\mathrm{A}\} = (a_1 \quad a_2 \quad \cdots \quad a_n)$ is weight coefficient row vector, *b* is constant. Substituting DIV into Eq.(21), the result *de* is the damage severity.

In summary, this cable damage identification approach should be separated into two identification machines, DCIM and DSIM. The flow chart of the damaged cable identification is shown in Fig.4.

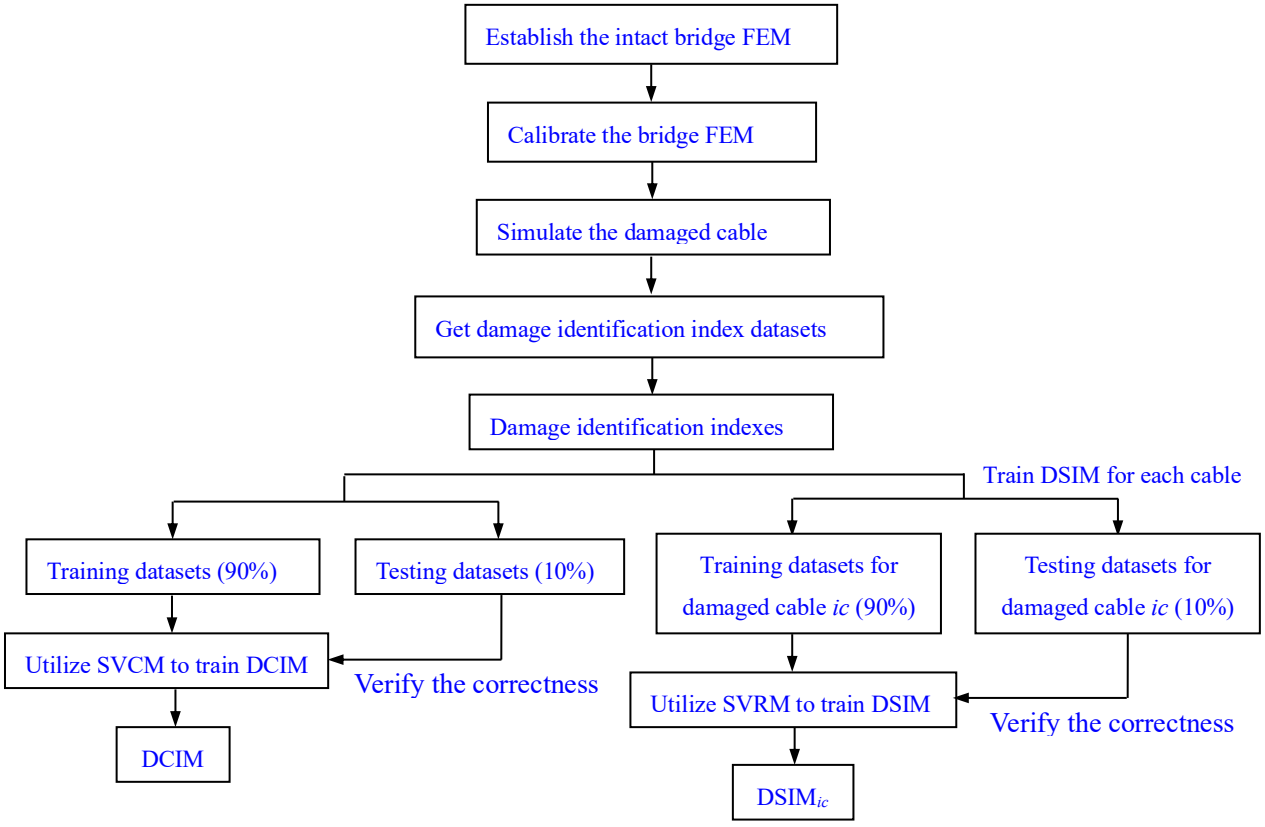

Fig.4 The flow chart of the damaged cable identification

3 The SHM system and FEM of the cable-stayed bridge

3.1 Description of the SHM system

A long-term monitoring system has been installed on a cable-stayed bridge as shown in Fig.5. There are 24 accelerometers on the bridge deck and their locations are indicated in Fig.5(a). The locations of the strain gauges are elaborated in Fig.5(b). All eight cables were instrumented with uni-axial strain gauges, denoted by SA*i*(*i* = 23 to 30) in Fig.5(b). Uni-axial strain gauges SU*i*(*i*= 17 to 22) were mounted

under the deck in either the longitudinal or transverse direction between Cross Girders CG6 and CG7. Strain gauges SU*i*(*i* = 13 to 16) were installed under the flange of the longitudinal girders at the middle of the span between CG6 and CG7 to measure bending strains. These strain gauges were also located close to mid-span of the bridge, where large deflections are expected. Shear rosettes were mounted at three different longitudinal locations along the bridge: the north end of the span near Cross Girder CG2, bridge mid-span close to Cross Girder CG6, mid-span close to Cross Girder CG6, and halfway between Cross Girders CG6 and CG7 (Alamdari et al. 2019). These strain gauges are implemented to collect shear, bending and tension strains to characterize passing traffics and to identify the vehicle gross and axle weights. The response signals of the bridge were collected at 600Hz.

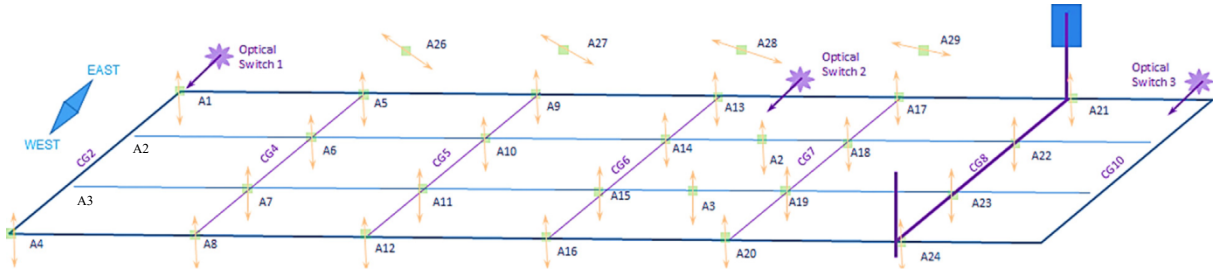

(a) Illustration of the accelerometer sensor locations (A1:A24) on the cross girders (CGs)

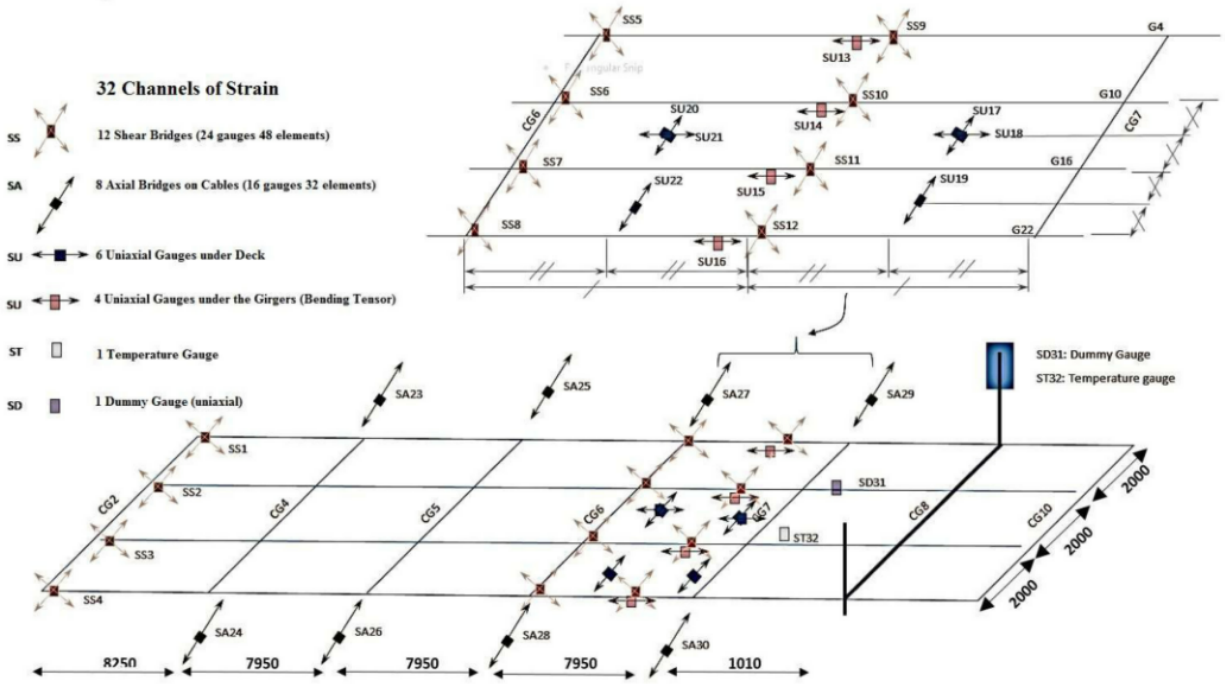

(b) Illustration of the strain gauges array

Fig.5 Illustration of the cable-stayed bridge SHM

3.2 FEM of the cable-stayed bridge

The Finite Element Model (FEM) of the cable-stayed bridge was established utilizing ANSYS. The bridge deck is a composite steel-concrete deck, so the steel reinforced concrete part is simulated by

SHELL63 with 160 mm thickness, the under longitudinal and transverse girders are simulated by BEAM189 which have Universal Beam (410UB54) cross sectional properties. These two kinds of elements are coupled at their co-nodes. The cables are super grade circular bar with a diameter of 38 mm and are all pre-tensioned cables using LINK10 to simulate. At the cable anchorage footing, all of the severities of freedoms are restrained. The bridge mast has a non-prismatic cross section, starting with a rectangular section of 700mm×800mm at the base and 500mm×800mm at the uppermost level. Consequently, in the cable-stayed bridge finite element model, BEAM189 with variable section is adopted to simulate the mast, and all severities of freedoms of the mast base are restrained. At abutment A (in Fig.2(c)), there is a pin support under every longitudinal deck. On the other side of the deck, roller supports are used at abutment B (in Fig.2(c)). The FEM of the cable-stayed bridge is shown in Fig.6.

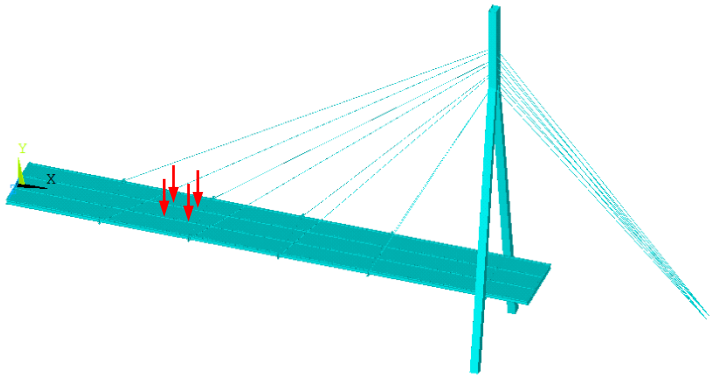

Fig.6 The FEM of the cable-stayed bridge under vehicle loads

3.3 Verification of the FEM

Based on the SHM system monitoring dynamic data, the FEM of the cable-stayed bridge is updated. In the FEM, some parameters are uncertain. For instance, because the cross girders have many circular openings for service ducts (in Fig.2(b)), their cross-section areas and moment of inertia are uncertain. And because the deck has reinforced steels and pavement, its density and modulus of elasticity are uncertain. An objective function can be established as,

$$f_1 = \mathrm{FEM}(A_\mathrm{c}, I_\mathrm{c}, E_\mathrm{d}) \tag{22}$$

where, f_1 is the monitoring first natural frequency. FEM() is the finite element model of the cable-stayed bridge. A_c and I_c are the updated cross section areas and moment of inertia of the cross girder, respectively. E_d is the updated modulus of elasticity of the deck. Since A_c and I_c are related to the cross-girder tension stiffness $E_\mathrm{c}A_\mathrm{c}$ and bending stiffness $E_\mathrm{c}I_\mathrm{c}$, its cross section can take the cross section of Universal Beam (410UB54), and only the modulus of elasticity E_c is modified. The objective function is simplified as

$$f_1 = \mathrm{FEM}(E_\mathrm{c}, E_\mathrm{d}) \tag{23}$$

Here, E_d=43.2 GPa, E_c=210 GPa.

Then the FEM modals and frequencies are calculated, and compared with the test data. Table 1 shows the first five FEM frequencies and the test frequencies (Sun et al., 2017). Fig.7 shows the first test mode shape and the first five mode shapes of the cable-stayed bridge.

Table 1 Frequencies from the finite element model and filed measurements

Mode No.	FEM Frequency (Hz)	Test Frequency (Hz) (Sun et al., 2017)	The difference (Hz)
1	2.038	2.014	0.024
2	3.163	3.510	-0.347
3	4.088	3.645	0.443
4	5.329	5.538	-0.209
5	6.530	6.068	-0.462

Note: the difference= FEM Frequency- Test Frequency

From Table 1, it can be found that the corresponding frequencies are close, and the maximum difference is -0.462 Hz, which is the fifth frequency. Fig.7 shows that the first FEM mode shape and the corresponding test mode shape (Zhu et al., 2017) are agreed well, and the mode's modal assurance criterion (MAC) is 0.9778, which is calculated by (Ghannadi et al., 2020a)

$$\mathrm{MAC}_i = \frac{\left|\{\emptyset_i^c\}^{\mathrm{T}}\{\emptyset_i^m\}\right|^2}{\left(\{\emptyset_i^c\}^{\mathrm{T}}\{\emptyset_i^c\}\right)\left(\{\emptyset_i^m\}^{\mathrm{T}}\{\emptyset_i^m\}\right)} \tag{24}$$

where, $\{\emptyset_i^c\}$ and $\{\emptyset_i^m\}$ denote the *i*th calculated mode shape and measured mode shape, respectively. When MAC_i is closer to 1, $\{\emptyset_i^c\}$ would fit well with $\{\emptyset_i^m\}$.

From these results, it is indicated that the FEM can represent the bridge global stiffness.

Furthermore, because this paper mainly uses the bending strain to obtain the damage identification indexes, the calculated bending strain is also compared with the measured bending strain to verify the FEM's correctness. The response measuring sensor is the SU15, which is located on the longitudinal deck just in between transverse beam CG6 and CG7 as indicated in Fig.5(b). In the field test experiment, a Holden Colorado Ute was used as a test vehicle, see Fig.8(a). The gross weight of the test vehicle was 2.2 t, with front and rear axle weights of P1 = 1.20 t and P2 = 1.00 t, respectively. The distance between the axles was d = 3.1m (Alamdari et al., 2019). The test vehicle was driving at approximately a constant speed of 10 km/h from the South to the North of the bridge along the centerline. Fig.8(b) illustrates the measured strain response (black line) and the FEM strain response (red line). The presence of two peaks, corresponding to two axles with front axle being heavier than the rear axle, can be clearly seen in both the measured and calculated bending responses in Fig.8(b). And these two lines are very close, the maximum values are almost the same. From the above, the FEM is validated.

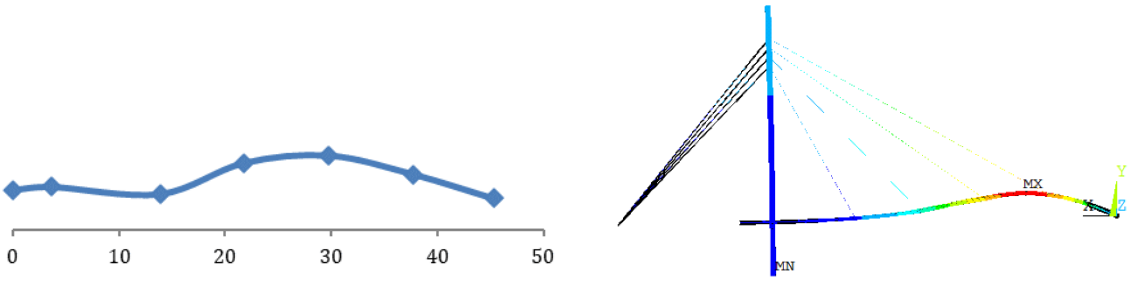

(a) The 1st test mode shape (Zhu et al., 2017) (b) The 1st FEM mode shape at side

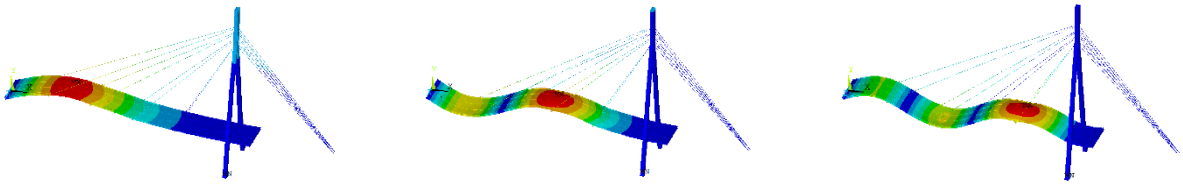

Mode 1: 2.039 Hz Mode 2: 3.301 Hz Mode 3: 4.254 Hz

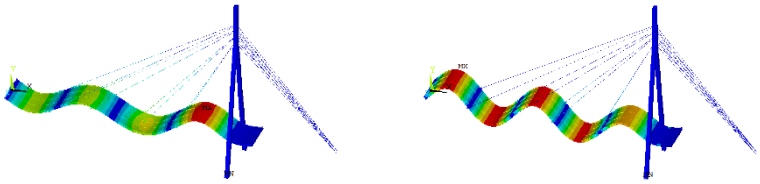

Mode 4: 5.329 Hz Mode 5:6.530 Hz

(c) The first five modes of 3D perspective

Fig.7 The mode shapes of the cable-stayed bridge

(a) Holden Colorado Ute

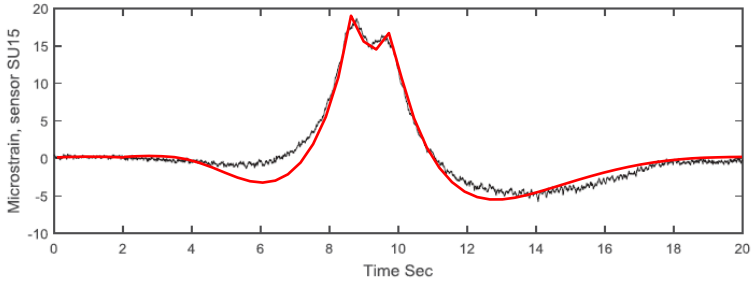

(b) The measured strain response (black line) and the FEM strain response (red line)

Fig.8 The test vehicle and the corresponding strains

4 Single cable damage identification

4.1The damage identification indexes

The damage identification indexes are obtained from the bending strain responses of the longitude deck which are near the cable anchor. The vehicle loads also used the Holden Colorado Ute which travels along the bridge centerline. Fig.9 shows the bending strain response under the cable 1-4 and cable 9-12 (Fig.2(c)), when the bridge is intact and the cable 4 is damaged 30%.

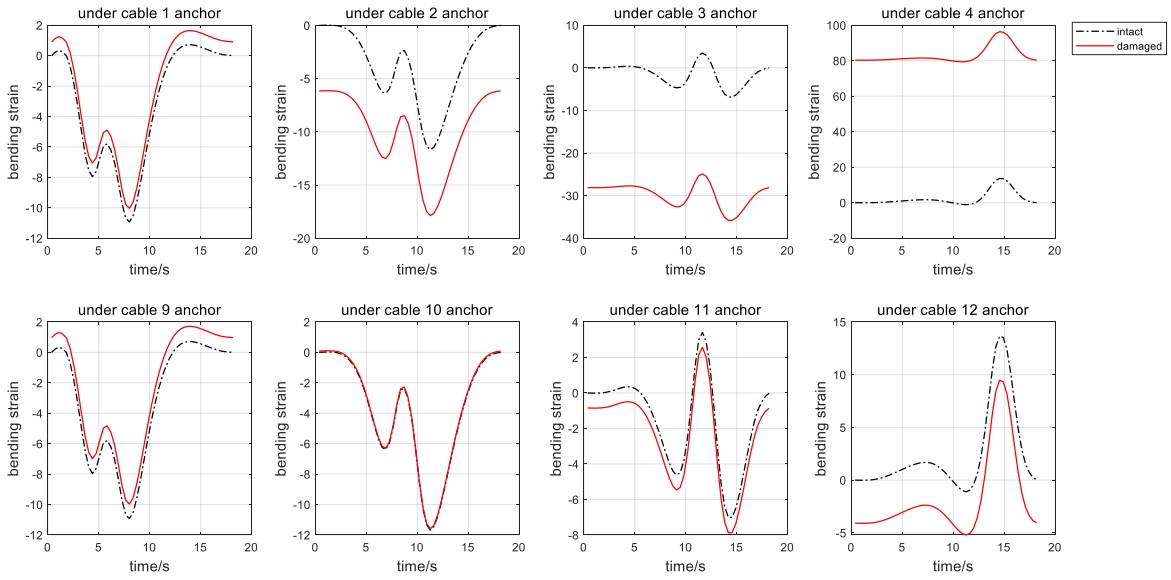

Fig.9 Bending strain response under the cable 1-4 and cable 9-12, when the bridge is intact and the cable 4 is damaged 30%

From Fig.9, it is obviously that the deck bending strain would be changed when the cable is damaged, especially near the damaged cable, such as the cable 4. But only according to these curve lines cannot identify the damaged cable or the damage severity. From Fig.9, for example, it is difficult to determine which cable is damaged, the cable 4 or the cable 3. Therefore, the new damaged identification approach in section 2.3 can be used to identify the damaged cable and its damage severity.

According section 2.3, corresponding to each cable anchor (cable 1-4, and cable 9-12), the difference between the maximum bending strains can be calculated by Eq.(19) to obtain a DIV, including 8 differences. Fig.10 shows the DIVs poly line diagrams when the cable 1-8 cross sections are reduced 30%, respectively. The measured points 1-8 are respectively under the cable anchors of cable 1-4 and cable 9-12. It indicates that the poly line diagrams are significant unique from each other when the cable1-4 are damaged, respectively. The poly line diagrams shapes of the cable 5-8 are similar, but each corresponding measured point values are different.

Furthermore, using FEM, when damage severity of the cable 4 are 10%, 20% and 30%, respectively, the corresponding DIV are calculated and their poly line diagrams are shown in Fig.11. It shows that the absolute values of damage identification index increase as the damage severity increases in cable 4, and their shapes are similar. Therefore, the cable damage severity identification can be considered as a regression problem.

4.2 Training datasets and testing datasets

Before training DCIM and DSIM, the training datasets and the testing datasets should be prepared firstly.

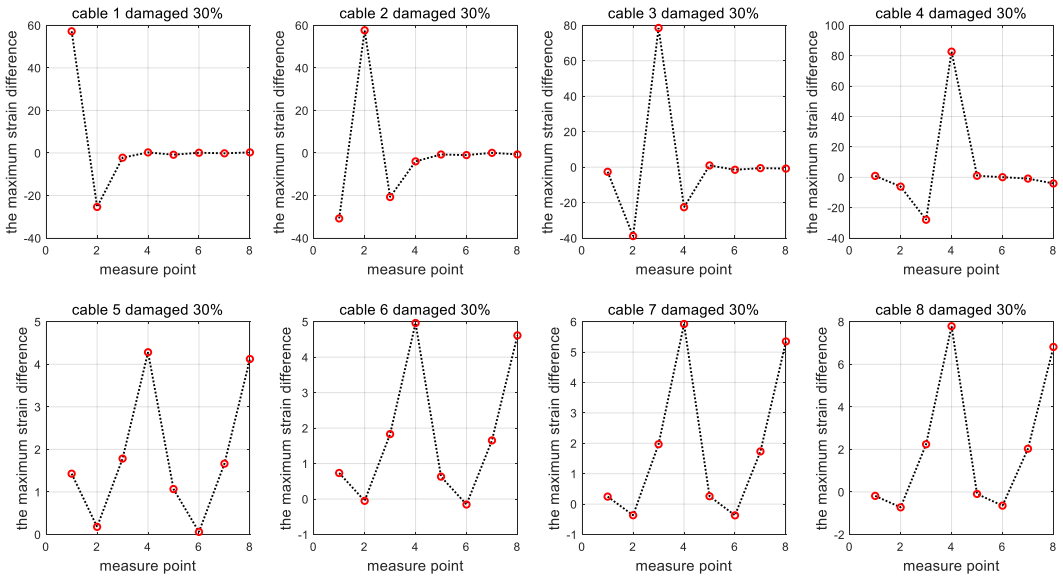

Fig.10 The DIV poly line diagrams when the cable 1-8 cross sections are reduced 30%

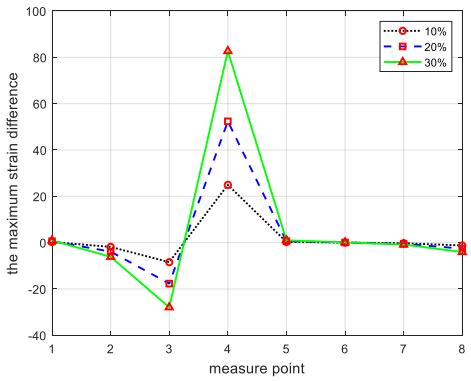

Fig.11 The DIV poly line diagrams when the cable 4 cross section is reduced 10%, 20% and 30%

(1) Training datasets

For ***the damaged cable identification***, the original training datasets $\{x\}^{ol}$ contains 16 DIVs, when the cable 1~16 are damaged 30%, respectively. So the corresponding damaged cable labels vector is $\{y\}^{ol}$=(1 2 3 … 16)$^{\mathrm{T}}$. In order to increase the number and the randomness of the training datasets, there are three steps to process the original datasets. First of all, the original datasets are expanded by Eq.(25) (Ren et al., 2013).

$$\begin{cases} \{x\}_{n\times 16}^{el} = \{x\}_{j}^{ol} \times (I_{n\times n} + \varepsilon \cdot \mathrm{diag}(R)_{n\times n}) \\ \{y\}_{n\times 1}^{el} = y_{j}^{ol} \times \mathrm{ones}_{n\times 1} \end{cases} \tag{25}$$

where, $\{x\}_{n\times 16}^{el}$ and $\{y\}_{n\times 1}^{el}$ are the expanded data vector of the jth original DIV and the corresponding damaged cable label vector, respectively. $\{x\}_{j}^{ol}$ and y_{j}^{ol} are the jth original DIV and the corresponding damaged cable label, respectively. $I_{n\times n}$ is the identity matrix. ε is the noise level. $\mathrm{diag}(R)_{n\times n}$ is a diagonal matrix, which diagonal component is a normally distributed random data with a mean of 0 and a mean square deviation of 1. $\mathrm{ones}_{n\times 1}$ is a vector with all components being 1. Here, n is 15 and ε is 0.1%, the number of original data is 16. After expanding, the number of samples is 240.

The second step is to add white noise into each component of the expanded training datasets by Eq.(26).

$$x_{ij}^{tl} = x_{ij}^{el} \times \left(1 + \varepsilon R_j\right)(j = 1,2,\cdots,m) \tag{26}$$

where, x_{ij}^{tl} and x_{ij}^{el} are the *j*th component of the *i*th training DIV and the *j*th component of the *i*th expanded vector. ε *and* R_i are same with the meaning in Eq.(25). Here, ε is 1%, m is 8 for the number of the measured points being 8.

At last, the training vectors should be normalized in [0,1] to increase the identification accuracy and reduce errors. In Matlab, it can be processed by the function "mapminmax ", and its algorithm is

$$f: x_{ij}^{tl} \to X_{ij}^{trl} = \frac{x_{ij}^{tl} - x_{ij\min}^{tl}}{x_{ij\max}^{tl} - x_{ij\min}^{tl}} \tag{27}$$

where, $x_{ij\min}^{tl}$ and $x_{ij\max}^{tl}$ are the minimum component and the maximum component of the vector x_i^{tl}, respectively. X_{ij}^{trl} is the normalized component. Then the training datasets $[X]^{\text{trl}}$ for the damaged cable identification is obtained, which is a 240×8 matrix.

For ***damage severity identification***, the cable 2 is taken as an example. The DIV are calculated using the former FEM, when the cable 2 damage severities are 10%, 20% and 30% respectively. The original damage severity identification training datasets $\{x\}^{od}$ only contains 3 DIVs and their poly line diagrams have shown in Fig.12. The damage severity vector is $\{y\}^{od}$=(10 20 30)$^{\text{T}}$. They also are added white noise to simulate measured datasets. In Eq.(25), n is 40 and ε is 1%, and the number of the expanded training datasets is 160. In Eq.(26), ε is 1%, m is 8. It must be mentioned that this training datasets do not need to be normalized. Finally, the number of the training samples $[x]^{\text{trd}}$ and the corresponding $\{y\}^{trd}$ are 160.

(2) Simulated measured datasets

In order to test DCIM and DSIM generalization capability and anti-noise capability, the hypothetical damage scenarios are listed in Table 2 to simulate measured (SM) datasets. DIVs in Table 2 are calculated by FEM.

Table 2 The hypothetical damage scenarios

	Damaged cable No.	Damage severity	Remarks	Damaged cable No.	Damage severity	Remarks
Damaged cable identification test scenarios	1	10%, 20%	Not included in the training datasets	10	25%	Not included in the training datasets
	2	10%, 20%, 25%		11	20%	
	3	10%, 20%		14	20%	
	4	10%, 20%				
Damage severity identification test scenarios	2	10%, 20%, 25%, 30%	25% is not included in the training datasets			

Then the damaged cable identification SM input dataset $[X]^{tel}$ includes 12 damage scenarios. The exact output vector is $\{y\}^{tel}=(1\ 1\ 2\ 2\ 2\ 3\ 3\ 4\ 4\ 10\ 11\ 14)^{T}$. The damage severity identification SM test input datasets $[x]^{ted}$ includes 4 damage scenarios, and output is $\{y\}^{ted}=(10\ 20\ 30\ 25)^{T}$. Then they are expanded by Eq.(25) to 80 damage scenarios, where n is 20 and ε is 0.01%.

At the following sections, the Support Vector Machine (SVM) will be utilized to train DCIM and DSIM, which are based on the above training datasets.

4.3 Damaged cable identification

It has been mentioned that the damaged cable identification is a multi-classification problem. And on the Matlab platform, the function "fitcecoc" fit multiclass models for SVCM. Therefore, this paper uses the function “fitcecoc” to train DCIM. The major training steps are as follows:

(1) $[X]^{trl}$ are randomly divided into two subsets: 90% of $[X]^{trl}$ is used for training DCIM, 10% of $[X]^{trl}$ is used for testing DCIM.

(2) Choosing the Gaussian kernel as the kernel function.

(3) Using function “fitcecoc” to train DCIM.

(4) Using function “crossva” to cross-validate DCIM using 10-fold cross-validation.

(5) Using function “kfoldLoss” to get classification loss for cross-validated DCIM, it’s 4% here.

Then $[X]^{tel}$ are input in DCIM to get identified damaged cable label $\{y\}^{pl}$. $\{y\}^{pl}$ and the actual damaged cables $\{y\}^{tel}$ are shown in Fig.12(a). Although $[X]^{tel}$ is not included in the training datasets, it can be observed from Fig.12(a) that the identified results are exactly correct. Since there are many disturbances in the field experiment environment, studying the anti-noise capability of DCIM is necessary. The following noise levels 5%, 10%, 20% are considered and added into $[X]^{tel}$ using Eq.(26). These noised SM datasets are input in DCIM and the identification results are show in Fig.12(b), (c), (d).

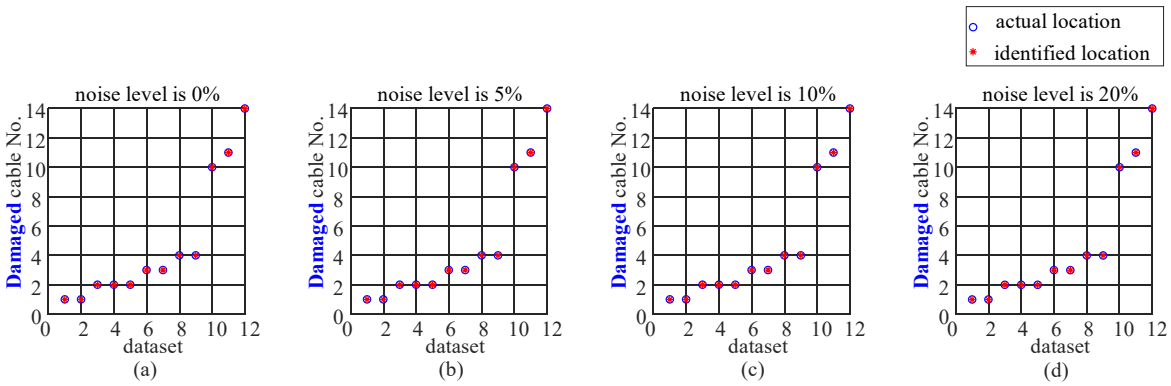

Fig.12 The comparison between the actual damaged cable and the identified damaged cable with different noise levels

From Fig.12, even the noise level is up to 20%, there is not any misidentified damaged cables. Obviously, DCIM has excellent anti-noise capability and good generalization capability, and the DIV are

also effective to identify the damaged cables.

4.4 Damage severity identification

After finishing the damaged cable identification, damage severity recognition will be studied in this part. At first, $[x]^{trd}$, which is obtained at section 4.2, is used to train DSIM by SVRM at Matlab platform. The major training steps are as follows:

(1) $[x]^{trd}$ and $\{y\}^{trd}$ are randomly divided into two subsets according the proportion 90% and 10%, $[x]_{90}$ and $\{y\}_{90}$ are used for training DSIM, $[x]_{10}$ and $\{y\}_{10}$ are used for testing DSIM.

(2) Using function "fitrsvm" to train DSIM by optimizing hyperparameters automatically, such as:

"*DSIM = fitrsvm(*$[x]_{90}$*, *$\{y\}_{90}$*, 'OptimizeHyperparameters', 'auto', 'HyperparameterOptimizationOptions', struct('AcquisitionFunctionName', 'expected-improvement-plus'))*"

(3) $[x]_{10}$ is input DSIM to get $\{y\}^{p}$, the codes are:

$$\{y\}^{p} = \text{predict(DSIM, } [x]_{10})$$

(4) The performance of DSIM is measured by mean squared error (*MSE*) (Ghannadi et al., 2021), regression correlation coefficient squared (R^2), uncertainty interval U95 and Reliability (Sabed-Movahed, F et al. 2020). The mathematical relations of these parameters are given in Eq.(28)-(31).

$$MSE = \frac{1}{N}\sum_{i=1}^{N}(P_i - D_i)^2 \tag{28}$$

$$R^2 = \frac{\sum_{i=1}^{N} {P_i}^2}{\sum_{i=1}^{N} {P_i}^2 - \sum_{i=1}^{N}(P_i - D_i)^2} \tag{29}$$

$$\text{U95} = \frac{1.96}{N}\sqrt{\sum_{i=1}^{N}(D_i - \overline{D})^2 + \sum_{i=1}^{N}(D_i - P_i)^2} \tag{30}$$

$$\text{Reliability} = \left(\frac{100\%}{N}\right)\sum_{i=1}^{N} k_i \tag{31}$$

where P_i is the identified damage severity, D_i is the exact damage severity, N is the number of samples, $\overline{D}$ is the mean value of the exact damage severity. k_i is obtained through two steps. First, the relative average error (*RAE*) is defined as a vector whose ith component is

$$RAE_i = \left|\frac{D_i - P_i}{D_i}\right| \tag{32}$$

Next, is $RAE_i \leqslant \Delta$, then k_i =1, otherwise, k_i =0, where Δ is the threshold value, it can be 0.1 or 0.05.

When the *MSE* is closer to 0, R^2 is closer to 1, U95 is closer to 0 and Reliability is closer to 100, DSIM would have a good performance. Here, *MSE* is 0.3468, R^2 is 1.0008, U95=0.1490, Reliability is 100 when Δ=0.1, or is 86.6667 when Δ=0.05.

Then $[x]^{ted}$ is input in the DSIM, and the output results are the damage severity of cable 2. Table 3 lists *MSE*, R^2, U95 and Reliability when the test data is added in different noise levels, such as 0%, 5%,

10%, 15%, 20%.

Table 3 The performance results of DSIM for *MSE*, R^2, U95 and Reliability

	Noise level	0%	5%	10%	15%	20%	Remarks
Damage severity of 10%	*MSE*	0.1787	0.1834	0.3640	0.3964	0.6550	Included in the training datasets
	R^2	1.0016	1.0017	1.0033	1.0037	1.0065	
	U95	0.1853	0.1877	0.2644	0.2760	0.3547	
	Reliability(Δ=0.1)(%)	100	100	90.00	95.00	80.00	
Damage severity of 20%	*MSE*	0.2357	0.4677	0.8801	2.3850	2.1926	
	R^2	1.0006	1.0012	1.0023	1.0066	1.0057	
	U95	0.2128	0.2997	0.4122	0.6768	0.6490	
	Reliability(Δ=0.1)(%)	100	100	90.00	80.00	80.00	
Damage severity of 30%	*MSE*	0.0679	0.6401	1.5673	6.1620	8.4525	
	R^2	1.0001	1.0007	1.0017	1.0070	1.0090	
	U95	0.1142	0.3506	0.5487	1.0879	1.2742	
	Reliability(Δ=0.1)(%)	100	100	100	90.00	65.00	
Damage severity of 25%	*MSE*	0.1199	0.4228	1.3951	3.0524	5.0408	Not included in the training datasets
	R^2	1.0002	1.0007	1.0023	1.0052	1.0085	
	U95	0.1517	0.2850	0.5177	0.7657	0.9840	
	Reliability(Δ=0.1)(%)	100	100	95.00	80.00	60.00	

From Table 3, with the noise level increasing, *MSE*, R^2 and U95 have a tendency to increase, but Reliability is decreasing. It indicates that DSIM performance is getting worse with the noise lever increasing. However, most of MSE are smaller than 6, except the situation of the damage severity of 30% with noise level 15% and 20%. All of R^2 are very close to 1, the maximum is only 1.0090. U95 is also smaller than 1.2742. When the noise level is less than 15%, the reliabilities are all above 80%. When the noise level is 20%, the reliabilities are also 80% of the damage severity of 10% and 20%. Although the damage severity of 25% is not included in the training datasets, DSIM still have good performance. Therefore, DSIM can well identify the damage severity, have good generalization capability and strong anti-noise performance. And these DIV, which are proposed in this paper, are effective to identify the cable damage severities.

5 Double damaged cables identification

In real situation, there may be two damaged cables simultaneously. The key steps are also to train the double damaged cable identification machine (DDCIM) and the double damage severity identification machine (DDSIM). The double cables DIVs are obtained by superimposed the single cable DIVs corresponding different damaged cables. In DDCIM, the categories include all the scenarios when any two cables are damaged simultaneously. Such as, when the total number of cables are *nn* in a cable-stayed bridge, the categories are $\sum_{i=1}^{nn-1} i$, which is more than that in DCIM. If the double damaged cables are identified, DDSIM needs to train for each cable damage severity separately.

5.1 The double damaged cables identification datasets

(1) Training datasets

For ***double damaged cables identification***, the double cables DIVs can be obtained as Eq.(33).

$$\begin{cases} \{x\}_k^{dol} = \{x\}_i^{ol} + \{x\}_j^{ol} \\ \{y\}_k^{dol} = (\{y\}_i^{ol} \quad \{y\}_j^{ol}) \end{cases} \quad (i \neq j, i = 1,2,\cdots,nn; j = 1,2,\cdots,nn; k = 1,2,\cdots,\sum_{i=1}^{nn-1} i) \quad (33)$$

Where, $\{x\}_k^{dol}$ and $\{y\}_k^{dol}$ are the *k*th DIV of the double damaged cables identification training datasets and the corresponding damaged cable labels, respectively. $\{x\}_i^{ol}$ and $\{x\}_j^{ol}$are respectively the *i*th and the *j*th single cable DIV, and $\{y\}_i^{ol}$ and $\{y\}_j^{ol}$are respectively the *i*th and the *j*th single damaged cable label, where *i* and *j* cannot equal to each other. *nn* is the total number of cables in the cable-stayed bridge, here *nn*=16. It also can be expanded and added noise by Eq.(25) and Eq.(26).

For ***double damaged cables damage severity identification***, different DSIMs should be trained for different damaged cables. The training datasets can be obtained as Eq.(34).

$$\begin{cases} \{x\}_k^{dod} = \{x_{cn}\}_i^{od} + \{x_{cm}\}_j^{od} \\ \{y\}_k^{dod} = (\{y_{cn}\}_i^{od} \quad \{y_{cm}\}_j^{od}) \end{cases} \quad (i = 1,2,\cdots,mm; j = 1,2,\cdots,mm; k = 1,2,\cdots,mm \times mm) \quad (34)$$

Where, $\{x\}_k^{dod}$ and $\{y\}_k^{dod}$ are the *k*th DIV of the double damaged cables damage severity identification training datasets and the corresponding damage severities. $\{x_{cn}\}_i^{od}$, $\{x_{cm}\}_j^{od}$ and $\{y_{cn}\}_i^{od}$, $\{y_{cm}\}_j^{od}$ are the *i*th and the *j*th single cable DIV and damage severity for cable *cn* and cable *cm*, respectively. *mm* is the number of the single damage severity scenarios, such as 10%, 20%, 30%, *mm*=3. They also can be added white noise to simulate measured datasets by Eq.(25) and Eq.(26).

(2) Testing datasets

In order to test the identification results of DDCIM and DDSIM, there are two hypothetical damage scenarios. In the scenario ①, cable 1 is damaged 10% and cable 2 is simultaneously damaged 20%. In the scenario ②, cable 1 is damaged 20% and cable 11 is simultaneously damaged 10%. The corresponding DIV are directly calculated by FEM and are added white noise by Eq.(26) to get the testing datasets $DATA_{td}$, the noise levels include 5%、10%、20%. For DDCIM, the actual output is $\{y\}_{test}^{dol} = \begin{pmatrix} 1 & 2 \\ 1 & 11 \end{pmatrix}$. For DDSIM, the actual output is $\{y\}_{test}^{dod} = \begin{pmatrix} 10 & 20 \\ 20 & 10 \end{pmatrix}$.

5.2 The double damaged cables identification

DDCIM is trained on the Matlab platform, and the training steps are same as the Section 4.3. Then, the testing datasets $DATA_{td}$ are input into DDCIM, the output $\{y\}_{id}^{dol} = \begin{pmatrix} 1 & 2 \\ 1 & 11 \end{pmatrix}$ is completely correct.

Although the training datasets are just obtained by superposition principle, DDCIM can exactly identify the damaged cables, even when the noise level is 20%. It is shown that the training datasets can be obtained by superposition principle based on single cable damage datasets for multiple damage scenarios, such as two cables damage or more. It also indicates that DDCIM has good anti-noise capability.

5.3 Damage severity identification

If damage scenario ② has been identified, the training datasets $\{x\}^{dod}$ can be obtained by Eq.(34), where *cn*=1, *cm*=11. DDSIM is trained by SVRM on Matlab platform, and the training steps can be find in Section 4.4. Then the testing DIV datasets about damage scenario ② is input into $DDSIM_1$ and $DDSIM_{11}$, respectively. The identified damage severity, the exact damage severity with different noise levels and the errors are all shown in Table 4.

Table 4 The double **damaged** cables damage severity identification results of damage scenarios ②

Noise level	The assumed damaged cable	The exact damage severity (%)	The identified damage severity (%)	error (%)
0%	1	20	19.21	-0.79
	11	10	10.08	0.08
5%	1	20	18.90	-1.10
	11	10	10.29	0.29
10%	1	20	18.18	-1.82
	11	10	10.66	0.66
20%	1	20	20.25	0.25
	11	10	8.86	-1.14

where, error = identified damge severity − exact damage severity

From Table 4, the identified damage severities are very close to the exact damage severities, the maximum error is just -1.82% of the damaged cable 1 with the noise level of 10%. When the noise level is lower than 20%, the identified error is less than 2%. This example also shows that the method of obtaining the training datasets using superposition principle based on single cable damage datasets for multiple damage condition is correct and can be used in real condition. DDSIM has good anti-noise capability.

6 Conclusions

Bending strain-based DCIM and DSIM have been developed to identify the damaged cable in a cable-stayed bridge. A cable-stayed bridge FEM is established using ANSYS, and validated by the field measurements. The validated FEM is used to generate the training and testing datasets for DCIM and DSIM. Some conclusions can be made as follows:

1) DCIM can accurately identify the single damaged cable from the bending strain measurements with

the noise level up to 20%. DSIM works well on identifying the damage severities, the maximum error is 4.9329% when the noise level is 20%. The identification results show that both DCIM and DSIM have the good generalization capability and anti-noise capability.

2) Based on the single damaged cable identification datasets, DDCIM and DDSIM are developed to identify double damaged cables. The results show that both DDCIM and DDSIM are accurate and robust to identify the double damaged cables. The identified error is less than 2% when the noise level is up to 20%.

3) The proposed method has strong anti-noise performance and can be easily adapted to the field health monitoring system. The scenarios with three or more damaged cables are much complicated to be discussed next step. The effect of the geometric nonlinearity and material nonlinearity need to be considered for practical application in the long-span cable-stayed bridges. Further study is needed to develop an integrating system for simultaneously identifying the damage in both the cable and bridge deck.

Acknowledgements

This research is supported by research funding of National Natural Science Foundation of China (NSFC) (11972238, 11902206) and the Australian Research Council Discovery Project (DP160103197). The financial aid is gratefully acknowledged.

References

Alamdari MM, Kildashti K, Samali B and Goudarzi HV (2019) Damage diagnosis in bridge structures using rotation influence line: Validation on a cable-stayed bridge. *Engineering Structures* 185: 1-14.

Arjomandi K, Araki Y and MacDonald T (2019) Application of a hybrid structural health monitoring approach for condition assessment of cable−stayed bridges. *Journal of Civil Structural Health Monitoring* 9: 217-231.

Brice SM, Ness KF, Rosemond D, Lyons K, Davis M (2008) Development and validation of a method to directly measure the cable force during the hammer throw. *Sports Biomechanics* 7(2): 274-287.

Bisheh HB, Amiri GG, Nekooei M, Darvishan E (2020) Damage detection of a cable-stayed bridge based on combining effective intrinsic mode functions of empirical mode decomposition using the feature selection technique. *Inverse Problems in Science and Engineering* 29(6): 861-881.

Carrión FJ, Quintana JA and Crespo SE (2017) SHM of a stayed bridge during a structural failure, case study: the Rio Papaloapan Bridge. *Journal of Civil Structural Health Monitoring* 7: 139-151.

Cho S, Jo H, Jang S, Park J, Jung HJ, Yun CB, Jr BFS. and Seo JW (2010) Structural health monitoring of a cable-stayed bridge using wireless smart sensor technology: data analyses. *Smart Structures and Systems* 6(5-6): 461-480.

Dong JL, Yan X and Li SL (2018) Cable force monitoring and prediction for cable group of long-span cable-supported bridges. *Journal of Civil Structural Health Monitoring* 8: 597-605.

Ghannadi P, Kourehli SS (2019a) Structural damage detection based on MAC flexibility and frequency using moth-flame algorithm. *Structural Engineering and Mechanics* 70(6): 649-659.

Ghannadi P, Kourehli SS (2019b) Model updating and damage detection in multi-story shear frames using Salp Swarm Algorithm. *Earthquakes and Structures* 17(1): 63-73.

Ghannadi P, Kourehli SS (2019c) Data-driven method of damage detection using sparse sensors installation by SEREPa. *Journal of Civil Structural Health Monitoring* (9): 459-475.

Ghannadi P, Kourehli SS (2020a) Multiverse optimizer for structural damage detection: Numerical study and experimental validation. *Structural Design of Tall and Special Buildings* 29(3): e1777.

Ghannadi P, Kourehli SS, Noori M and Altabey WA (2020b) Efficiency of grey wolf optimization algorithm for damage detection of skeletal structures via expanded mode shapes. *Advances in Structural Engineering* 23(13):2850-2865.

Ghannadi P, Kourehli SS (2021) An effective method for damage assessment based on limited measured locations in skeletal structures. *Advances in Structural Engineerin*g 24(1): 183-195.

Hasni H, Alavi AH, Jiao PC, Lajnef N (2017) Detection of fatigue cracking in steel bridge girders: A support vector machine approach. Archives of Civil and Mechanical Engineering 17(3): 609-622.

Huang YH, Wang Y, Fu JY, Liu A and Gao W (2018) Measurement of the real-time deflection of cable-stayed bridge based on cable tension variations. *Measurement* 119: 218-228.

Kim SW, Jeon BG, Cheung JH, Kim SD and Park JB (2017) Stay cable tension estimation using a vision-based monitoring system under various weather conditions. *Journal of Civil Structural Health Monitoring* 7: 343-357.

Kim SW, Jeon BG, Kim NS and Park JC (2013) Vision-based monitoring system for evaluating cable tensile forces on a cable-stayed bridge. *Structural Health Monitoring* 12(5-6): 440-456.

Kourehli SS (2020) Damage Identification of Structures Using Second-Order Approximation of Neumann Series Expansion. *Journal of Rehabilitation in Civil Engineering* (8-2): 81-91.

Kourehli SS (2017) Structural damage diagnosis using incomplete static responses and LS-SVM. *Inverse Problems in Science and Engineering* 25(3): 418-433.

Li H, Huang Y, Chen WL, Ma ML, Tao DW, Ou JP (2011) Estimation and warning of fatigue damage of FRP stay cables based on acoustic emission techniques and fractal theory. *Computer-Aided Civil and Infrastructure Engineering* 26 (7): 500-512

Li H and Ou JP (2016) The state of the art in structural health monitoring of cable-stayed bridges. *Journal of Civil Structural Health Monitoring* 6: 43-67.

Li H, Ou JP and Zhou Z (2009) Applications of optical fibre Bragg gratings sensing technology-based smart stay cables. *Optics and Lasers in Engineering* 47: 1077-1084.

Li XK, Guo YC, Li YM (2020) Particle Swarm Optimization-Based SVM for Classification of Cable Surface Defects of the Cable-Stayed Bridges. *IEEE ACCESS* 8: 44485-44492.

Mehrabi B (2006) In-service evaluation of cable-stayed bridges, over-view of available methods and findings. *Journal of Bridge Engineering ASCE* 11(6): 716-724.

Najafzadeh M, Ghaemi A(2019a) Prediction of the five-day biochemical oxygen demand and chemical oxygen demand in natural streams using machine learning methods. *Environmental Monitoring and Assessment* 191(6): 380.

Najafzadeh M, Etemad-Shahidi A, Lim SY(2016) Scour prediction in long contractions using ANFIS

and SVM. *Ocean Engineering* 111: 128-135.

Najafzadeh M, Oliveto, G(2020) Riprap incipient motion for overtopping flows with machine learning models. *Journal of Hydroinformatics* 22(4): 749-767.

Najafzadeh M, Zeinolabedini, M(2019b) Prognostication of waste water treatment plant performance using efficient soft computing models: an environmental evaluation. *Measurement* 138: 690-701.

Nazarian E, Ansari F and Azari H (2016a) Recursive optimization method for monitoring of tension loss in cables of cable-stayed bridges. *Journal of Intelligent Material Systems and Structures* 27(15): 2091-2101.

Nazarian E, Ansari F, Zhang XT and Taylor T (2016b) Detection of tension loss in cables of cable-stayed bridges by distributed monitoring of bridge deck strains. *Journal of Structural Engineering* 142(6): 04016018.

Pan H, Azimi M, Yan F, Lin ZB (2018) Time-Frequency-Based Data-Driven Structural Diagnosis and Damage Detection for Cable-Stayed Bridges. *Journal of Bridge Engineering* 23(6): 04018033

Ren JY, Su MB and Zeng QY (2013) Damage identification of railway simply supported steel truss bridge based on Support Vector Machine. *Journal of Applied Sciences* 13(17): 3589-3593.

Ren Y, Xu X, Huang Q, Zhao DY and Yang J (2019) Long-term condition evaluation for stay cable systems using dead load-induced cable forces. *Advances in Structural Engineering* 22(7): 1644-1656.

Sim SH, Li J, Jo H, Park JW, Cho S, Jr BFS and Jung HJ (2014) A wireless smart sensor network for automated monitoring of cable tension. *Smart Materials and Structures* 23: 025006 (10pp).

Son H, Pham VT, Jang Y and Kim SE (2021) Damage localization and severity assessment of a cable-stayed bridge using a message passing neural network. *Sensors* 21, 3118.

Sun M, Alamdari MM and Kalhori H (2017) Automated operational modal Analysis of a cable-stayed bridge. *Journal of Bridge Engineering ASCE* 22(12): 05017012.

Sun ZK, Li GM, and Geng SH (2013) Study on stayed-cable health monitoring. In: *Proceedings of Intelligence Computation and Evolutionary Computation*, AISC, Berlin: 1091-1098.

Vapnik VN (1998) Statistical Learning Theory. Wiley, New York.

Wang G and Ye J (2019) Localization and quantification of partial cable damage in the long-span cable-stayed bridge using the abnormal variation of temperature-induced deck deflection. *Structural Control Health Monitoring* 26(1): e2281.

Yin SH and Tang CY (2011) Identifying cable tension loss and deck damage in a cable-stayed bridge using a moving vehicle. *Journal of Vibration and Acoustics* 133(April): 021007.

Zejli H, Gaillet L, Laksimi A, Benmedakhene S (2012) Detection of the presence of broken wires in cables by acoustic emission inspection. *Journal of Bridge Engineering* 17(6): 921-927.

Zhu XQ, Samali B, Rashidi M and Alamdari MM (2017) Long-term vibration monitoring of a cable-stayed bridge: effects of environmental and operational conditions. In: *Proceedings of the 8th International Conference on Structural Health Monitoring of Intelligent Infrastructure*, pp. 1132-1138.